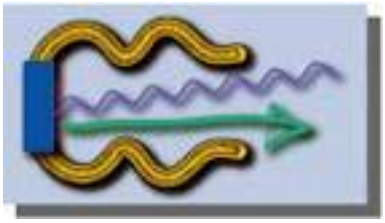

PHIN
A Joint Research Activity for Photoinjector

Deliverable N°2006-14

SRF GUN TEST REPORT

Jochen Teichert, André Arnold, Torsten Kamps, Petr Murcek, Rong Xiang

FZ Dresden-Rossendorf, Dresden, Germany

Abstract

Within the CARE project a superconducting RF photo electron gun (SRF gun) has been developed and installed at the superconducting CW linac of the radiation source ELBE. This report presents the results of the first measurement period of the SRF gun. The first cool-down of the SRF gun cryomodule took place in August 2007. The first electron beam was produced in November 2007 with a Cu photo cathode. Since May 2008 cesium telluride photo cathodes have been in use. The report contains the results of cryogenic and radio frequency measurements, the parameters of the UV driver laser and photo cathodes, and presents the beam parameter measurements.

CONTENT

1. Introduction

The report contains the results of the first measurement period of the superconducting RF photo electron gun which has been developed and installed at the superconducting CW linac of the radiation source ELBE [1]. The injector comprises the 3½ cell niobium cavity, the liquid He cryomodule, the RF supply system, the support, cooling and exchange system for the photocathodes, the UV driver laser with its optical beamline, a solenoid for emittance compensation downstream the gun, and a diagnostic beamline. The SRF gun uses normal conducting photocathodes which are thermally separated from the cavity and cooled with liquid nitrogen. The standard material is Cs_2Te. A photograph of the SRF gun installed in the ELBE accelerator hall is presented in Fig. 1.1. Details of the SRF gun design were published elsewhere [2].

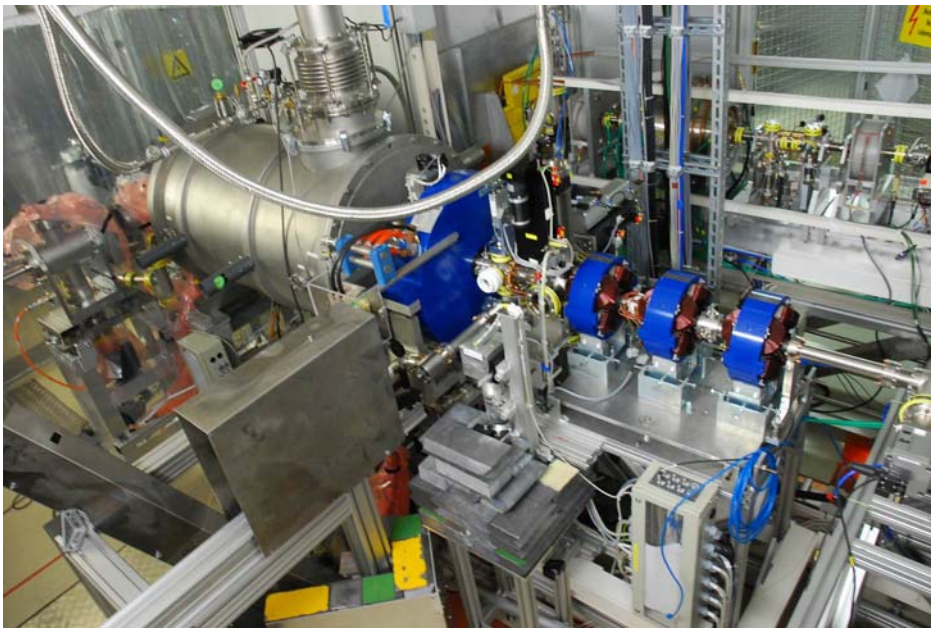

Fig. 1.1: Photograph of the superconducting RF photo gun (SRF gun) in the ELBE accelerator hall.

The SRF gun cryomodule was installed in July and the first cool-down was performed in August 2007. In the following weeks the RF system was put into operation. At the same time the driver laser system was delivered by MBI and tested, and the optical components of the laser beamline were installed and adjusted. The autumn shut-down of ELBE was used to complete the installation of the diagnostics beam line. End of October, the gun was cooled down for the second time. After readjustment of the laser beamline the first accelerated beam could be produced on November 12, 2007. The electrons were extracted from a Cu photocathode. Fig. 1.2 shows the first beam recorded on the first YAG screen of the diagnostics beam line. The time until end of 2007 was spent for commissioning and test of the beamline components. In March 2008 the cathode transfer system was completely mounted and the first Cs_2Te photo cathodes were inserted into the gun. From May until September 2008 the gun was operated with these photo cathodes.

Since November 2007 the gun was operated for about 500 hours without serious problems. Thereby the beam time with Cs_2Te photo cathodes was about 400 hours. The gun was

operated in parallel to the user operation of the ELBE accelerator. The average current was mostly about 1 µA and always less than 10 µA due to radiation safety restrictions. During the beam time the acceleration gradient was always 5 MeV/m which belongs to 13.5 MV/m peak field in the cavity and about 4.5 MV/m at the photo cathode. The liquid helium consumption due to RF power input was about 5 W.

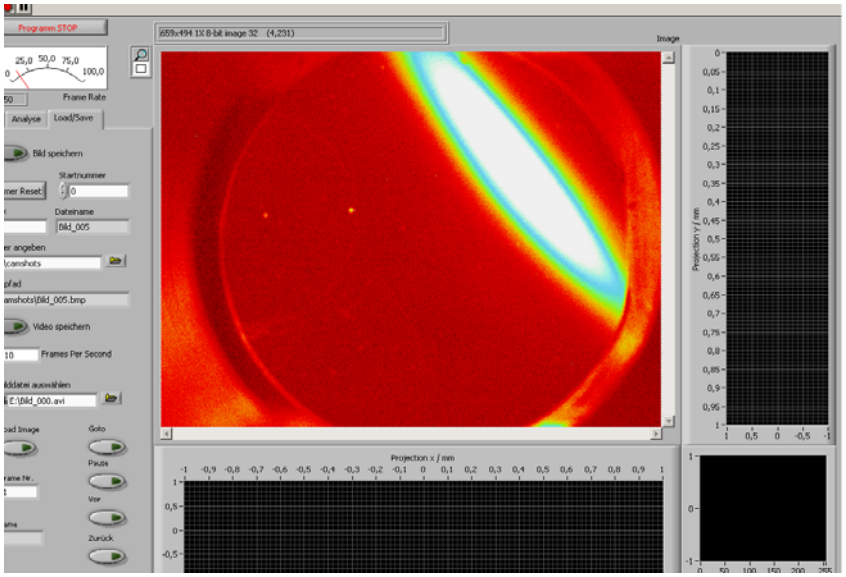

Fig. 1.2: First beam of the SRF gun on November 12th, 2007. The beam spot is visible on a YAG screen in the diagnostics beam line.

2. Cryomodule

The design of the SRF gun cryomodule is shown in Fig. 2.1. The module comprises the 3½ cell superconducting niobium cavity in the centre. The cavity is welded into the He tank which is made of titanium. Behind the half-cell of the cavity the superconducting choke filter is situated which mechanically belongs to the cavity. In the cavity half-cell the photo cathode is placed. The photo cathode is normal conducting and isolated from the Nb cavity by a circular vacuum gap. A special support system holds and cools the photo cathode with liquid nitrogen. From outside it is also possible to move and align the photo cathode with respect to the cavity. For that reason, three rotation feed-throughs exist in the backside plate of the vacuum vessel. On the left side on the end tube of the cavity the HOM couplers and the flange for 1.3 GHz main power coupler can be seen. The beamline vacuum tube on the left side is also used for incoupling of the UV laser beam. The vacuum tube on the right side is for photo cathode exchange. The cavity has two sets of tuners, one for the three TESLA cells, and one for the half-cell. The large vessel in the upper part of the module is the storage for the liquid nitrogen. Two circular tubes deliver the liquid N_2 to the cryogenic shield. Between cryogenic shield and the vacuum vessel, a magnet shield is located. More details of the cryomodule can be found in Ref. [3].

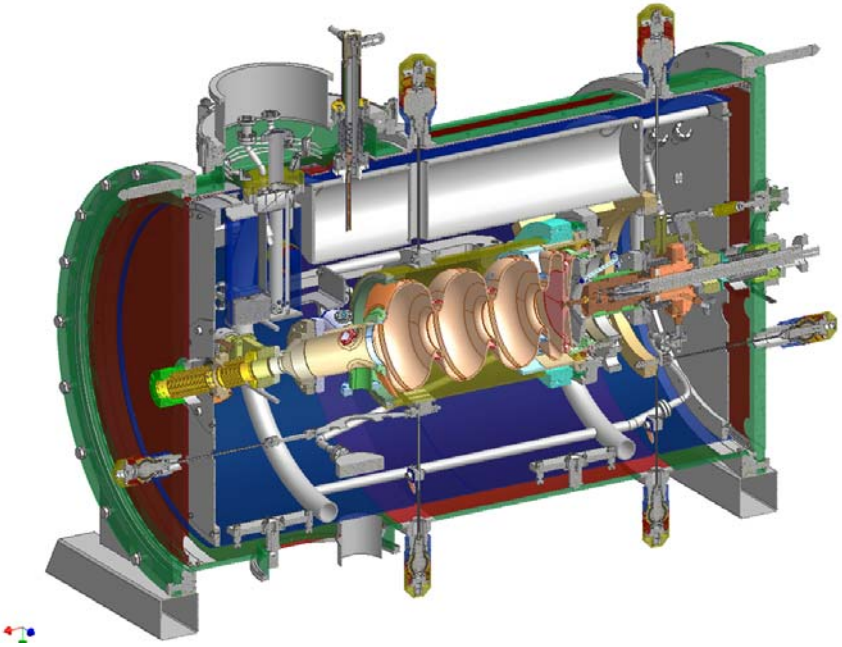

Fig. 2.1: Design of the SRF gun cryomodule.

The first cool-down of the SRF gun took place in August, 2007. For cooling and filling with liquid nitrogen two days were needed. Then the cavity was cooled down with He gas (10 K) for about 24 h. After a break in which the two ELBE modules were cooled with He gas, the tank was filled with liquid He. Finally, the tank was pumped to 30 mbar in order to get the working temperature of 2 K. Pressure stabilization is performed with cold compressors for all three cryostats of ELBE together using a pressure sensor near the first ELBE cryomodule. During the cool-down, the frequency of the π-mode (acceleration mode) was monitored as it is shown in Fig. 2.2. For the frequency shift from RT to 2 K a value of 2.02 MHz was found which is equal to the shift of TESLA resonators in the ELBE cryomodules. Unfortunately, the pre-stress adjustment of the SRF gun tuners was wrong. Thus, the final frequency obtained is about 400 kHz higher than expected.

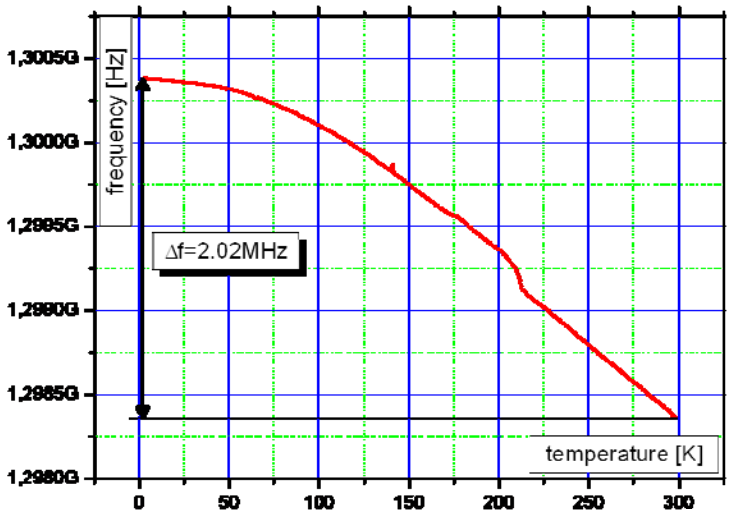

Fig. 2.2: Cool-down curve of the SRF gun cryomodule: cavity resonance frequency versus temperature. The final temperature was 2.0 K.

The static He heat load of the cryomodule was determined from boil-off measurement. The curves in Fig. 2.3 show the liquid He level in the cryomodule after a shut-off (at t = 0) of the liquid He supply. The liquid helium content at 100 % level of the cavity tank is about 15 l. It needs about 110 min until the tank is empty. During that time the liquid N_2 cooled cryogenic shield was in use. In Fig. 2.4 the same boil-off curve is compared with a simulation using the 3D design data of the cryomodule and a temporally constant heat input. The best fit delivers a static heat load of 6 W.

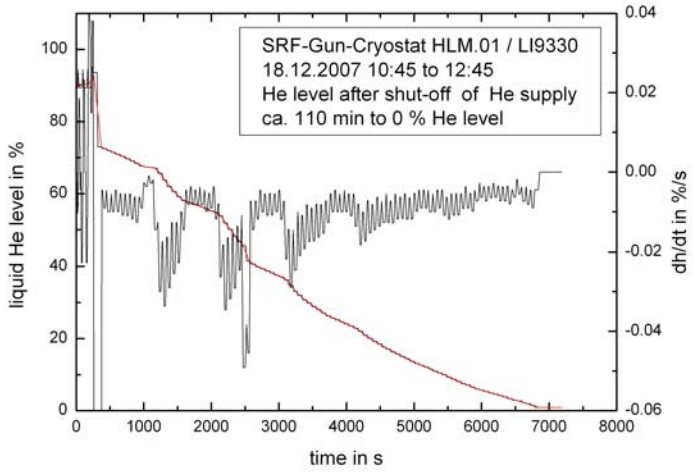

Fig. 2.3: Boil-off curve of the SRF gun cryomodule. The red curve (left scale) shows the He level in the tank as function of time after shut-off of the supply. The black curve is the time derivative (right scale).

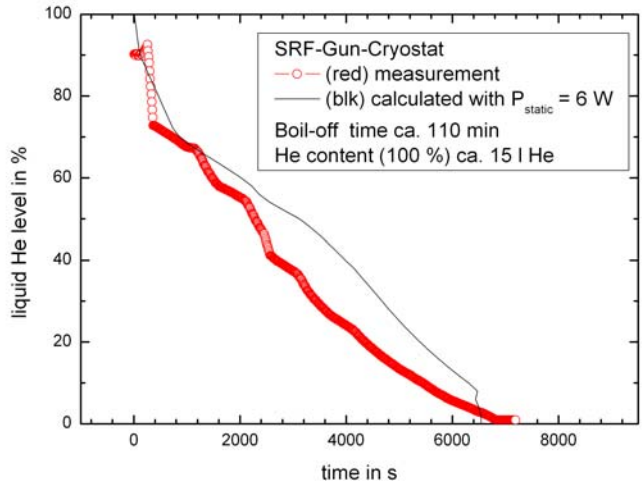

Fig. 2.4: Measured boil-off curve of the SRF gun cryomodule (red circles) and calculation (black curve) as function of time after shut-off of the supply. The black curve is a calculation using the 3D design data and a temporally constant heat input of 6 W.

Tab. 2.1: Parameters of the SRF gun cryomodule.

Parameter	**Value**	**Unit**
Total length of the vessel	1.3	m
Diameter of the vessel	0.75	m
Liquid He content	15	l
He working temperature	2.0	K
He working pressure	31	mbar
Cryogenic shield temperature (liquid N2)	77	K
Isolation vacuum pressure	10^{-6}	mbar
Power coupler vacuum pressure	10^{-7}	mbar
Beam line vacuum	$<10^{-8}$	mbar
He static heat load	6	W
N2 heat load	3 [1)]	l/h
He level stability	0.3	%
He pressure stability	0.1	mbar
Electric heater power	≤ 50	W

[1)] design value, not measured up to now.

3. RF measurements

3.1 Cavity performance measurement

The SRF gun cryostat has an electrical heater in the helium tank. For regular operating conditions, the liquid He flowing into the cryostat is constant. The different consumption due to variations of the acceleration gradient is compensated by adequate changes of the heater power. It is controlled by a level sensor in the He tank. Therefore the change of the heater power between switched-off RF at a given gradient is equal to the RF loss of the cavity. These values were measured as function of the acceleration gradient E_{acc}. The on-axis peak field E_{peak} in the cavity is related to the acceleration gradient by a factor of 2.7, i.e. $E_{peak} = 2.7 \times E_{acc}$. For the curve Q_0 versus E_{acc} the results in Fig. 3.1 are obtained. In the figure the second measurement on September 19, 2007 and the eighth measurement on August 28, 2008 are compared. For the second measurement the red curve shows the corresponding radiation level caused by field emission in the cavity. It is obvious that the drop down of Q_0 is connected to the field emission. There is no difference between the two measured Q_0 versus E_{acc} curves, i.e. about 500 h beam time with Cu and Cs_2Te cathode did not cause a degradation of the cavity.

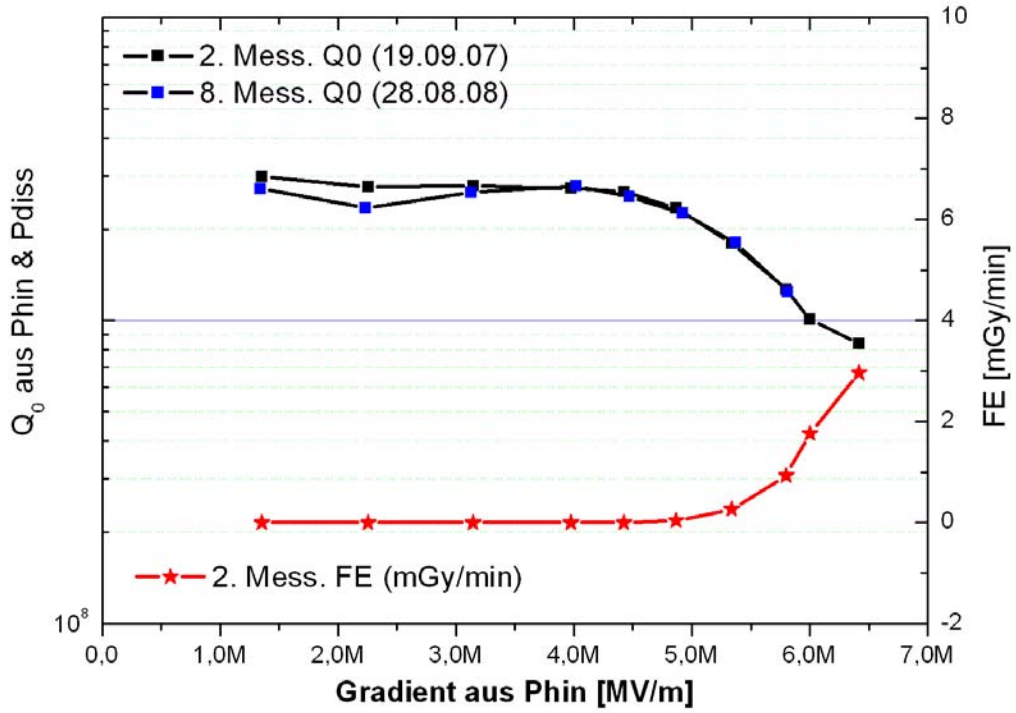

Fig. 3.1: Unloaded quality factor Q_0 versus acceleration gradient and corresponding field emission dose (right side). The figure shows the 2nd measurement in September 2007 and the 8th measurement in August 2008.

3.2 Passband and on-axis field distribution

Under the consideration of cool-down shrinking, change of permittivity and final BCP cleaning, the field distribution of the operated cavity inside the module can be calculated

using the fundamental mode pass band frequencies at 2 K and the last known cavity state before final cleaning. The four pass band mode frequencies measured in the gun at 2 K are shown in Fig. 3.2. In a mathematical model the RF properties of the 3½-cell cavity can be described by an eigenwert problem. The eigen values are the pass band resonance frequency and the eigen vectors are the field amplitudes in the four cell. Thus the field profile can be calculated from the measured frequencies. The obtained field distribution, shown in Fig. 3.3, is in very good agreement with the design values (64%, 100%, 100%, 100%).

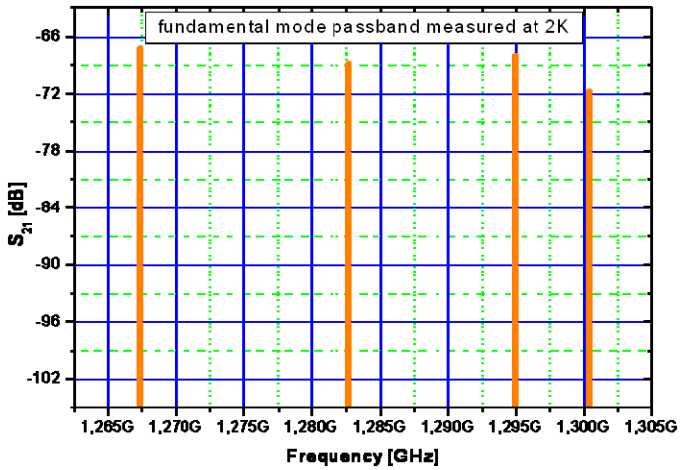

Fig. 3.2: Pass band mode measurement of the 31/2-cell cavity in the gun at 2 K.

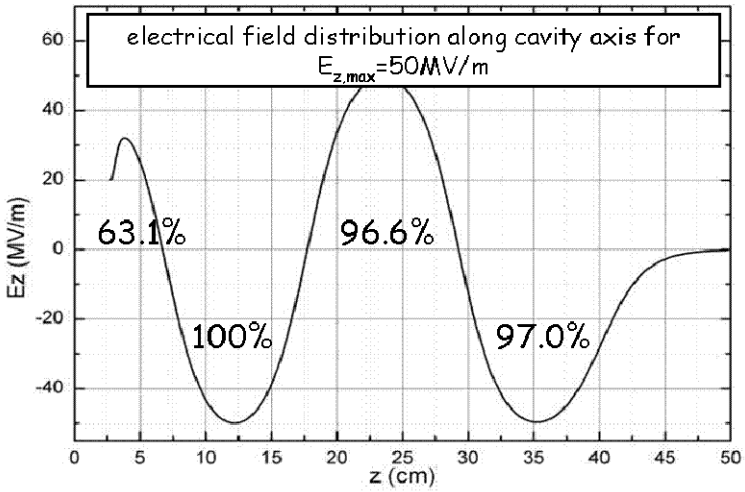

Fig. 3.3: Acceleration field distribution in the cavity at 2 K obtained from the pass band mode measurement. In the figure the distribution $E_z(z)$ is normalized to 50 MV/m peak field.

3.3 Pressure Sensitivity

In order to estimate the pressure sensitivity of the cavity, the resonant frequency and the pressure of the helium liquefier were measured at the same time for 12 hours. The result is shown in Fig. 3.4. Apparently, there are frequency peaks that are not correlated with the pressure in helium system but they occur at the same time when the liquid nitrogen shielding is filled. We guess that the amount of gaseous nitrogen during the first time of the filling

process is increasing the pressure in the feed pipe of the shielding, which probably results in detuning effect on the cavity. For the first test operation this is not a limiting fact, because the filling cycle is in the order of 3-4 hours. To eliminate this influence some design modifications will be implemented during the next warm up and modification phase in the third quarter next year.

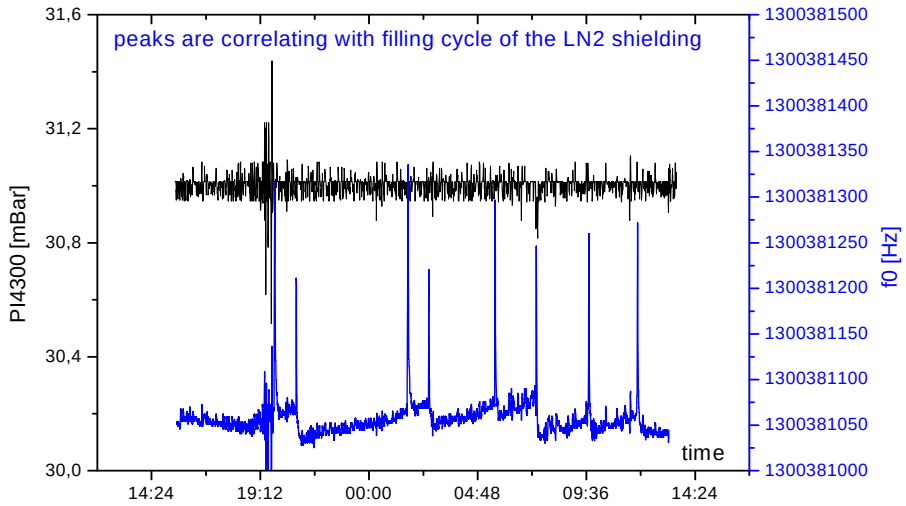

Fig. 3.4: Time domain plot of the resonant frequency and the helium pressure.

In order to get the pressure dependence of the resonant frequency, some minutes of the time domain frequency signal are plotted versus the pressure variation at the same time. The following linear fit function gives us a slope of approximately SR=230 Hz/mbar (see Fig. 3.5).

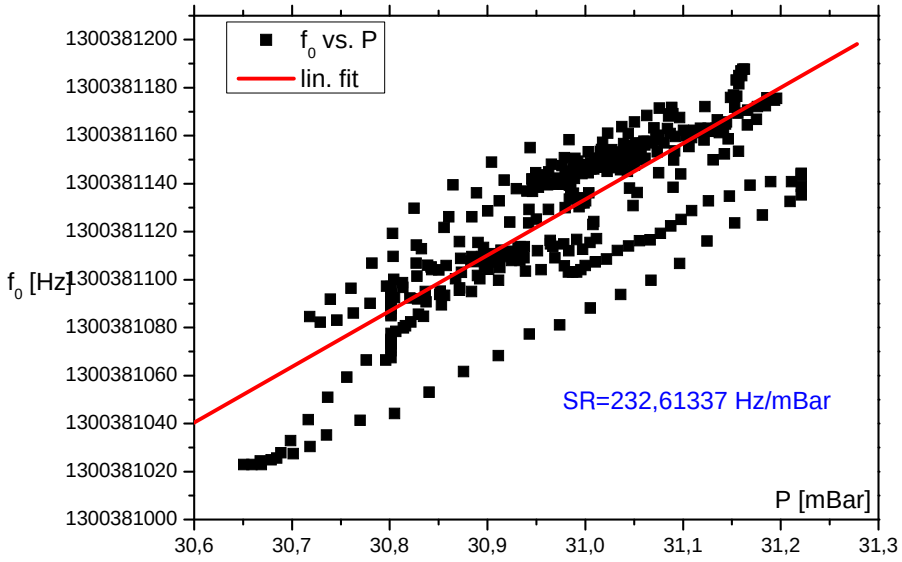

Fig. 3.5: f_0 vs. helium pressure with fitted straight line.

In comparison to the measured value of SR = 35Hz/mbar for the ELBE modules, the value is eight times higher. This could be a problem for operations at a high level of dissipated power which causes slow oscillations of the helium pressure and thus the phase controller could exceed its regulation limit. Beside additional design modifications of the cavity itself, also a control loop using the phase signal and the forward power as process variable and the cavity tuner as actuator could be used to improve the frequency behavior.

3.4 Lorentz Force Detuning

In order to measure the Lorentz force detuning of the SRF-Gun cavity, a network analyzer (NWA) was used as a driver unit for the klystron amplifier. Due to the fact that an increasing RF field is detuning the frequency downward, the NWA has to sweep the klystron from higher frequencies over the cavity resonance to lower values. Otherwise the maximum field could not be reached. To increase the cavity field, the output power of the NWA was raised in steps of 1dB while the gradient was calculated by the calibrated pickup voltage. The achieved typical resonance curves are shown in Fig. 3.6.

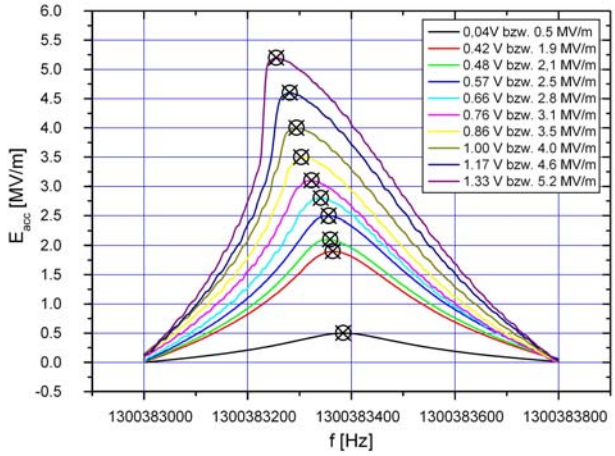

Fig. 3.6: Measurement of the transmitted signal S_{21} for increasing gradients.

If the frequency shift on crest is plotted versus the applied effective acceleration field in the cavity (cp. Fig. 3.7) one can find a quadratic dependence which can be explained by the radiation pressure that is proportional to quadratic field components

$$p_{rad} \propto \mu_0 H^2 - \varepsilon_0 E^2$$

and thereby the frequency shift is caused by deformation in a similar way (ref. 2).

$$\Delta f \propto \left(\varepsilon_0 E^2 - \mu_0 H^2\right) \Delta V$$

The determined constant of proportionality can be found to be

$$\Delta f = K \cdot x^2 \quad ; \quad \mathrm{K} = -5 Hz / \left(MV / m\right)^2$$

In order to compare the result with TESLA resonators used in the ELBE modules, the value must be referred to the peak field: K_{peak}= 0.69 $(MV/m)^2$. For the TESLA resonators this value is 0.25 $(MV/m)^2$ [4], i.e. the detuning of the SRF-Gun is about three times higher. The reason is the mechanical weakness of the half cell. At present, for gradients of E_{acc} = 5-6 MV/m the frequency shift is in the order of one bandwidth and causes no operational problems.

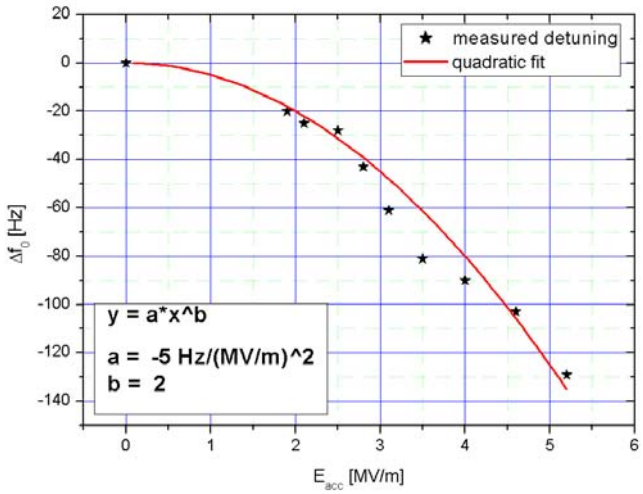

Fig. 3.7: Measured frequency shift Δf versus acceleration gradient.

3.5 High power processing

High power RF processing (HPP) of the SRF gun cavity has been carried out at the end of the first measurement period in September 2008. Due to the risk connected to this treatment it was scheduled to be at the end of the measurement period. It was hoped that this treatment could increase the cavity performance. Indeed, the HPP with pulsed RF up to E_{peak} = 25 MV/m results in a stable CW operation up to 17.6 MV/m peak field (E_{acc} = 6.5 MV/m). Above this level the cavity starts to quench. The improvement is demonstrated in Fig. 3.8 which shows the Q_0 versus E_{peak} curves before (2nd and 8th measurement) and after HPP (9th measurement). The higher gradient allows operating with 3 MeV particle energy in the next run.

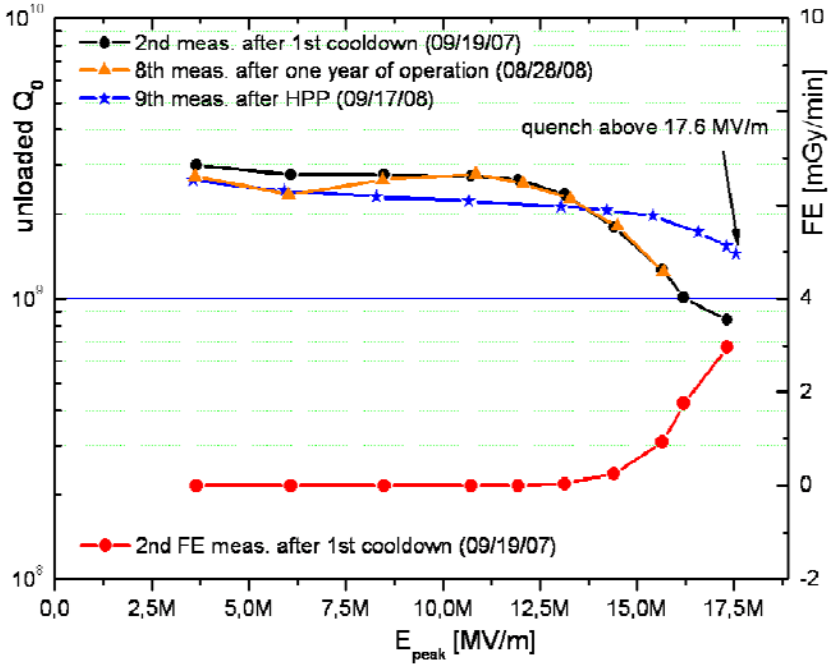

Fig. 3.8: Comparison of the cavity performance, unloaded quality factor Q_0 versus peak field E_{peak}, before and after high power RF processing of the cavity in September 2008.

4. Photo cathodes

During the commissioning of the SRF gun and the first test and measurement period from August 2007 until October 2008 two types of photo cathodes were used: a metallic copper cathode and later semiconductor cesium telluride (Cs_2Te) photo cathodes. In Table 4.1 a summary of the cathodes and their parameters are given. A more detailed description is given in the CARE report Ref. [5].

4.1 Cu photo cathode

The copper photo cathode consists of a massive polycrystalline Cu plug. The surface was polished to optical finishing and finally cleaned with citric acid. This photo cathode was mounted into the cavity during the assembly of the cryomodule in summer 2007. It was used during the first commissioning phase of the gun until the cathode transfer system was installed.

The Cu photo cathode was in use from October until December 2007. In October 2007 it was used for laser alignment experiments with a DC voltage applied. An electron beam was produced with this cathode from November 2007. The cathode was irradiated with the UV laser with 0.4 W power at 100 kHz repetition rate (4 µJ pulse energy). The quantum efficiency Q.E. was about 1×10^{-6}, which was rather low. However, an electron beam could be produced and observed on YAG screens. The laser cleaning for Q.E. improvement was not carried out.

4.2 Cs_2Te photo cathodes

After installation of the cathode transfer system, the first set of Cs_2Te photo cathodes for the SRF gun was produced in May 2008 in the preparation lab at FZD. After preparation the cathodes had quantum efficiencies of 4-5 × 10^{-2}. The first Cs_2Te cathode (#090508Mo) was in operation for 44 h until the ELBE shut-down in June 2008. Whereas its Q.E. was 4 % after preparation, it dropped down to 0.05 % after transfer to the SRF gun. Laser irradiation was typically with 50 mW at 100 kHz repletion rate. This cathode and all the others of the first set were damaged due to an accidental air of the transportation chamber during the shut down.

A second set of Cs_2Te photo cathodes was prepared and transported to the SRF gun in July 2008. The cathode #070708Mo was installed in the gun and was in operation until the end of the measurement period. Its Q.E. after preparation was 3 %. Again the Q.E. measurement in the SRF gun after insertion delivers a much lower value of about 0.1 %. Although the vacuum of 10^{-9} mbar in the transportation chamber was now good enough the worse vacuum during cathode exchange in the transfer chamber causes the drop-down of Q.E. Nevertheless the Q.E. was sufficient to produce bunch charges up to 200 pC and to conduct the beam parameter measurements of the SRF gun. The QE measurement was regularly repeated without any further significant changes during the whole measurement period.

The cathode cooling and support system worked properly. The cooling of the cathode with liquid nitrogen was efficient and a temperature increase of the photo cathodes was not observed.

The remote-controlled cathode alignment system was tested. But the parameter measurements were carried out only at one cathode position (about 2.5 mm retracted cathode). A cathode position variation and optimization will be carried out in the next beam time in 2009.

Tab. 4.1: Photo cathodes in use during the SRF gun commissioning from August 2007 until October 2008.

Cathode	Material	Q.E. in gun	max. bunch charge	operation period	operation hours
#001Cu	Cu	1×10^{-6}	0.5 pC	12.11.07 – 18.12.07	~100
#090508Mo	Cs2Te	5×10^{-4}		23.05.08 – 23.06.08	44
#070708Mo	Cs2Te	1×10^{-3}	200 pC	21.07.08-19.09.08	~350

As desired the photo cathodes can be exchanged without warming-up. Therefore the exchange needs less than 30 min.

At present, the main problem is the insufficient vacuum pressure in the transfer system. Because of the three-shift user operation of ELBE a short-term improvement could not be performed. It is intended to improve the vacuum pressure in the transfer system to $< 10^{-9}$ mbar until the next run in 2009. Additional NEG pumps will be installed and the vacuum chambers will be baked out for sufficient long time.

5. Drive laser

In order to fulfill the requirements of the SRF gun specifications, a UV laser system with two channels has been developed by MBI. The first channel will deliver laser pulses with 13 MHz repetition rate and 5 ps pulse length. For the second channel the maximum pulse rate is 500 kHz and the pulse length 15 ps. The two channels have different oscillators, but jointly used amplifier and UV conversion. At present, the 500 kHz channel is installed and used for the experiments. The frequency-quadrupled Nd:YLF system for CW operation consists of a mode-locked oscillator with 26 MHz, a regenerative amplifier, and a two-stage frequency conversion (LBO and BBO). The Pockels cells in the amplifier allow variable repetition rates up to 500 kHz of the output pulses. For 125 kHz and 2 kHz (diagnostic mode) the maximum pulse energies measured at 263 nm are 0.8 µJ and 50 µJ, respectively. A bunch charge of 1 nC requires 0.5 µJ pulse energy for a typical quantum efficiency of 1 %. The laser has a Gaussian temporal beam shape with a width of 15 ps FWHM.

In the first operation period of the gun with the Cu photo cathode the spatial shape was also Gaussian with a spot diameter of about 1.3 mm FWHM. For the present measurements the laser beam spot is enlarged changing the telescope on the laser table. Then the beam is cut with an aperture to obtain a circular flat top profile. A picture of the laser spot (virtual cathode) is shown in Fig. 5.1. The diameter of the spot is 2.7 mm.

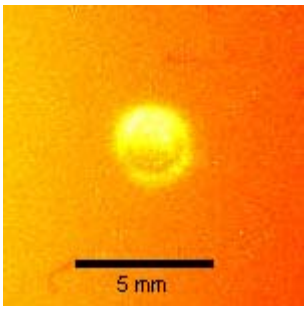

Fig. 5.1: CCD camera image of the laser spot at the virtual cathode. The spot diameter is 2.7 mm.

The optical transport system comprises four lenses, five dielectric mirrors, a beam splitter (virtual cathode) near the input port of the gun, and one metallic mirror inside the vacuum tube. The last dielectric mirror is remote controlled and used for laser positioning onto the cathode or scanning for local Q.E. measurements. With the virtual cathode the shape and position of the laser spot are monitored by means of a CCD camera and a position sensitive detector. A movable mirror in the electron beamline and a CCD camera provide a view onto the cathode. Together with a special luminescence cathode the laser beam can be adjusted.

The laser position stability was measured by means of the camera of the virtual cathode. From a series of pictures the centers of the laser spot were determined for each picture as shown in Fig. 5.2. The variation measured was 20 µm. A summary of the laser parameter is given in Table 2.1.

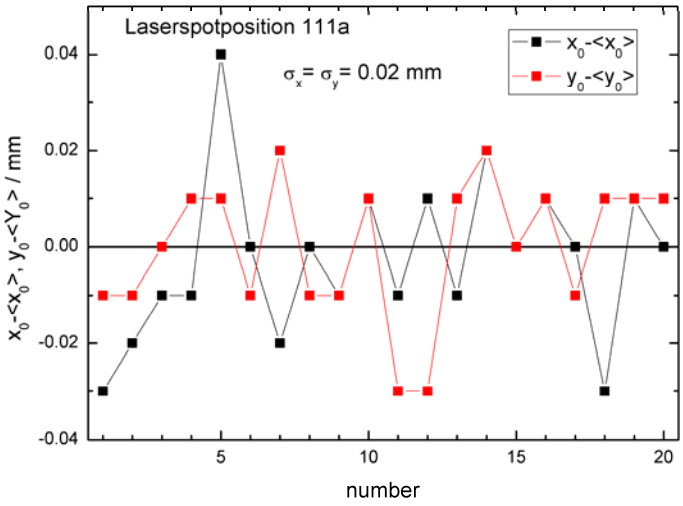

Fig. 5.2: Measured laser spot centroid jitter at the virtual cathode.

Together with a special luminescence cathode the laser beam was adjusted. Laser beam alignment, difficult at begin, later much simpler due to special alignment cathode & without cathode

Tab. 2.1: Parameters of the SRF gun UV driver laser (500 kHz module).

Parameter	**Value**	**Unit**
UV wave length	263	nm
Spot diameter on cathode (edge)	2.7	mm
Relative energy stability	< 5	%
Pulse duration (FWHM)	15	ps
Timing jitter with repect to RF (rms)	< 3	ps
x and y centroid jitter (rms)	20	µm
UV power on laser table	≤400	mW
UV energy on laser table	≤100	µJ
Repetition rate	1 - 500	kHz

6. Beam parameter measurements

The layout of the SRF gun diagnostic beam line beam for parameter measurements is shown in Fig. 6.1. For beam spot measurement the view screens (YAG) DV01 (Screen1), DV02 (SC 2), DV03 (Screen 3), DV04 (SC 4), and DV05 (Screen 5) are used. Beam current was measured with a Faraday cup at the position of screen 1 and with beam dump 1. The energy and energy width were measured with a 180° dipole magnet (C Bend) and screen DV05. For the transverse emittance measurements the solenoid and the screens DV01 or DV02 were used. A detailed description of the beam line is published [6].

The first step consists in a check of the laser spot position on the photo cathode and of the position of the gun solenoid. The laser spot has to be aligned with respect to the RF field axis of the cavity which can be proved by an RF phase or gradient variation and an observation of the e-beam spot on the following view screen. Thereby the gun solenoid is switched off. The alignment is correct if the e-beam spot remains on its position. The position accuracy of the solenoid is checked in a similar way by varying its current.

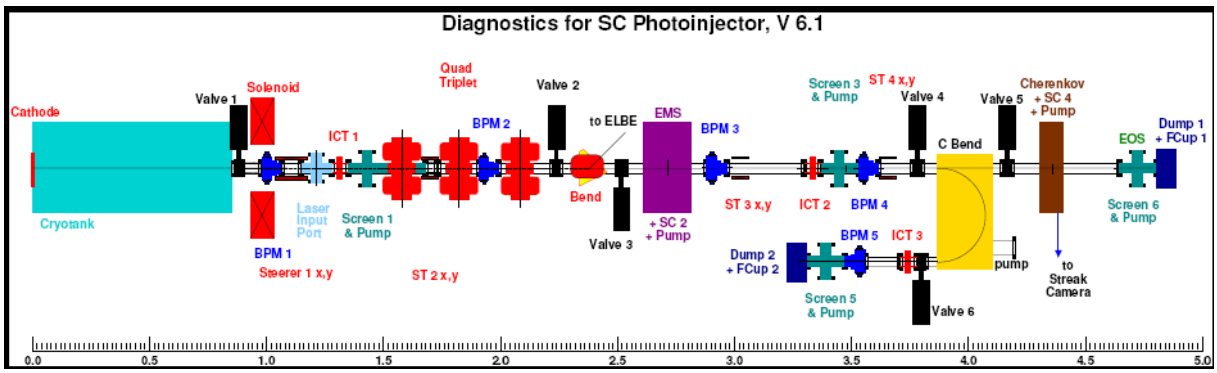

Fig. 6.1: Layout of SRF gun diagnostics beam line.

All beam parameter measurements were carried out with the following parameters:

Acceleration gradient: 5 MV/m,
Temporal laser pulse: Gaussian 15 ps FWHM,
Lateral laser spot on cathode: radial flat top with 2.7 mm diameter,
Photo cathode: ca. 2.5 mm retracted, 5 kV DC voltage,
Pulse repetition rate: CW with 1 – 125 kHz.

6.1 Laser phase scan (Schottky scan)

In a laser or Schottky scan the laser phase is varied with respect to the RF phase while measuring the accelerated bunch charge after the gun in a Faraday cup at constant laser pulse energy. In Fig. 6.2 such a measurement is shown for the whole phase range from -180° to 180°. In our definition the accelerating RF field is given by $B_z(z) = B_{z0}(z)\sin\varphi_{RF}$ and the z-axis corresponds to the beam direction. Due to the negative charge, electrons are emitted in the phase range -180° to 0°, whereas emission is suppressed in the phase range 0° - 180°. This behavior is clearly seen in the measured curve. The curve delivers important information on synchronization, phase jitter, and proper operation of the laser system. But the main purpose of the measurement is to determine the optimum laser launch phase for the operation of the gun.

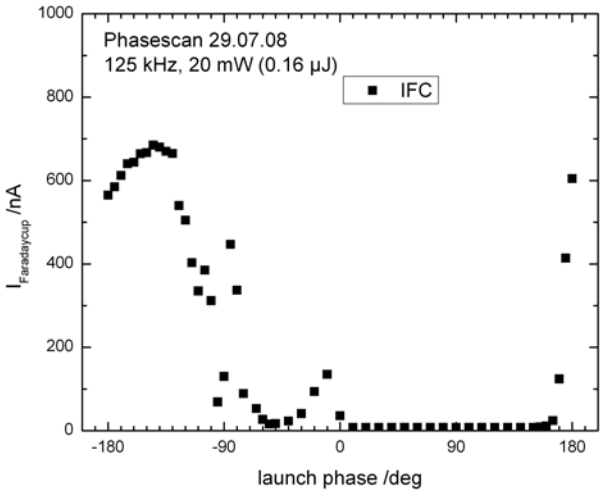

Fig. 6.2: Laser phase scan with low bunch charge measured for a full RF period from -180° to 180° (T = 1/f = 769.2 ps). The dark current measured in the phase range between about 0° and 180° is 8 nA.

This measurement has been carried out for different laser pulse repetition rates from 125 kHz down to 1 kHz with nearly the same laser power of 20 mW for each scan. The results for the interesting phase range from -180° to 0° are shown in the Figures 6.3 – 6.7. Whereas the average current is about the same, the bunch charge is increasing with lower laser pulse rate. In the 125 kHz case (Fig. 6.3) the shape curve is most pronounced. The increase of the current between -190° and -170° belongs to the zero-crossing point of the RF field. The slope is determined by the laser pulse length. For the operation of the gun the phase range between -180° and -110° can be used. Although not of interest for operation, the three peaks at -100°, -75°, and 0° have a physical nature. Simulations show that they belong to bunches which are created in one RF period, partly decelerated, and again accelerated and extracted out of the cavity in the following RF period. With increasing laser pulse energy (lower laser rep rate) and corresponding higher electron bunch charge, the space charge effect in front of the cathode becomes important. As visible in the figures, this effect smoothes the curve structures for higher bunch charges.

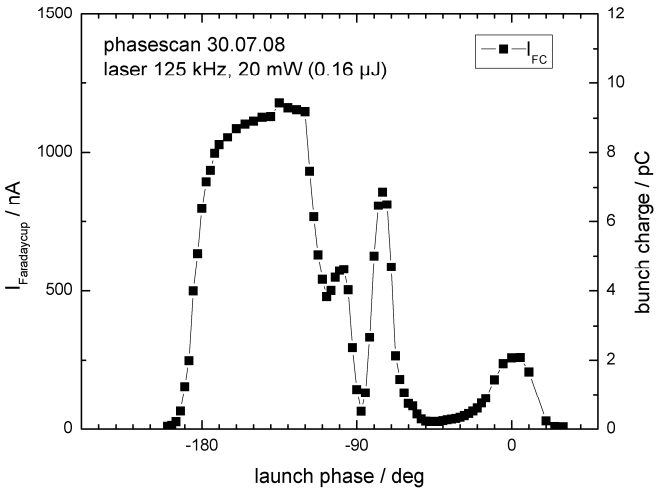

Fig. 6.3: Laser phase scan with 125 kHz laser pulse rate and 0.16 µJ pulse energy.

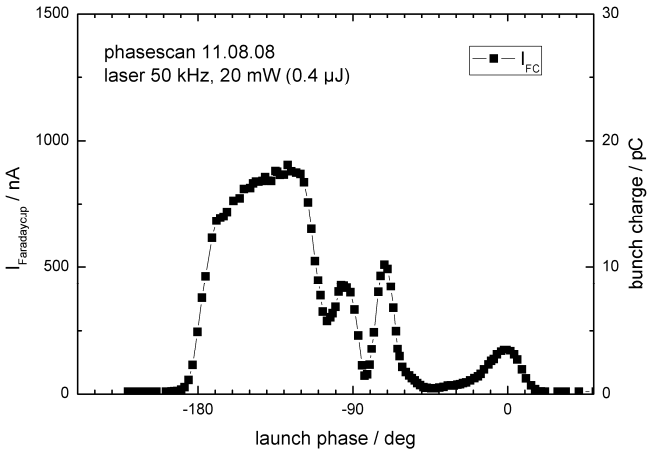

Fig. 6.4: Laser phase scan with 50 kHz laser pulse rate and 0.4 µJ pulse energy.

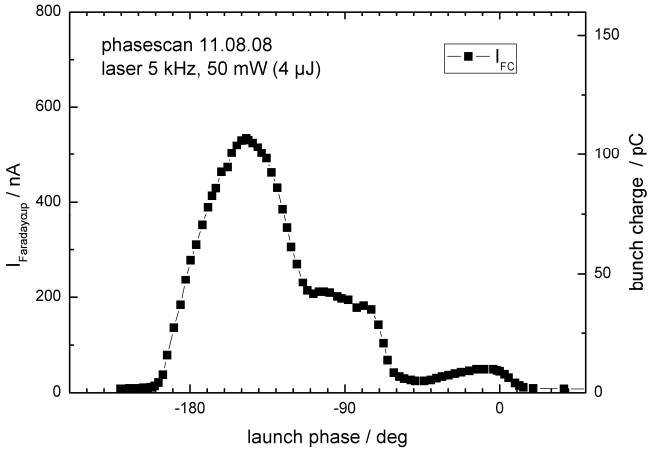

Fig. 6.5: Laser phase scan with 5 kHz laser pulse rate and 4 µJ pulse energy.

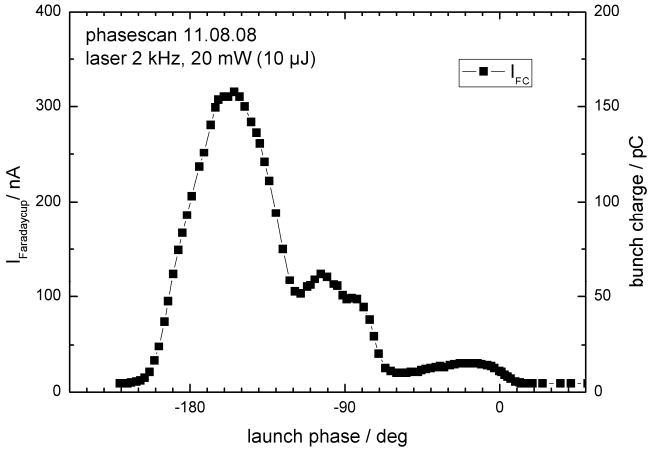

Fig. 6.6: Laser phase scan with 2 kHz laser pulse rate and 10 µJ pulse energy.

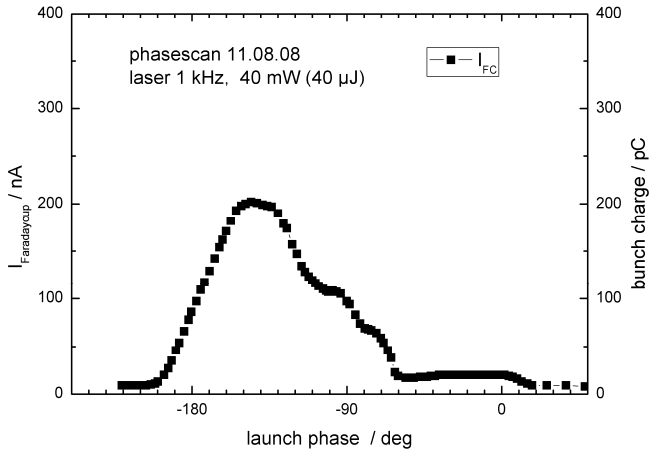

Fig. 6.7: Laser phase scan with 1 kHz laser pulse rate and 40 µJ pulse energy.

The Fig. 6.8 presents the electron beam images at the YAG screen DV02 obtained during the laser phase scan measurement with 50 kHz laser repetition rate and 20 mW laser power.

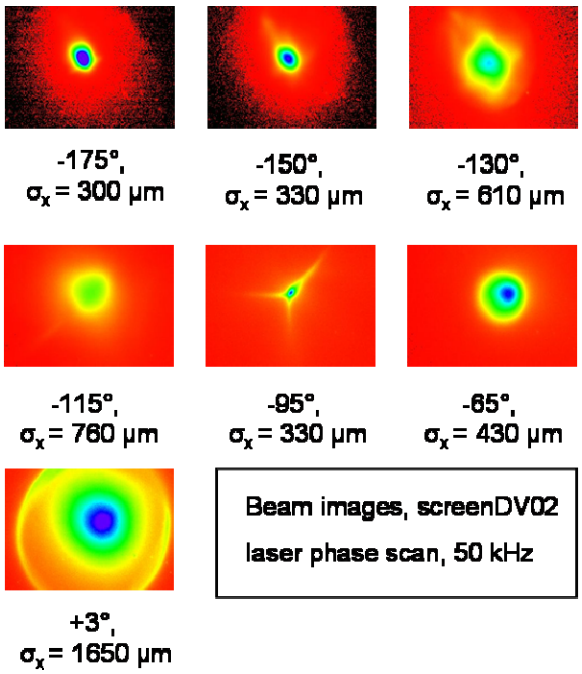

Fig. 6.8: Beam images at screen DV02 (YAG) belonging to the laser phase scan at 50 kHz (see Fig. 6.4). The values below the images are the corresponding phase and the rms beam size.

The measured bunch charges as function of laser phase for the different repetition rates are summarized in Fig. 6.9. Except the space charge smoothing the behavior is independent of the laser repetition rate. It confirms the proper synchronization of the laser and is important for further gun parameter optimization which thus carried out at low average currents.

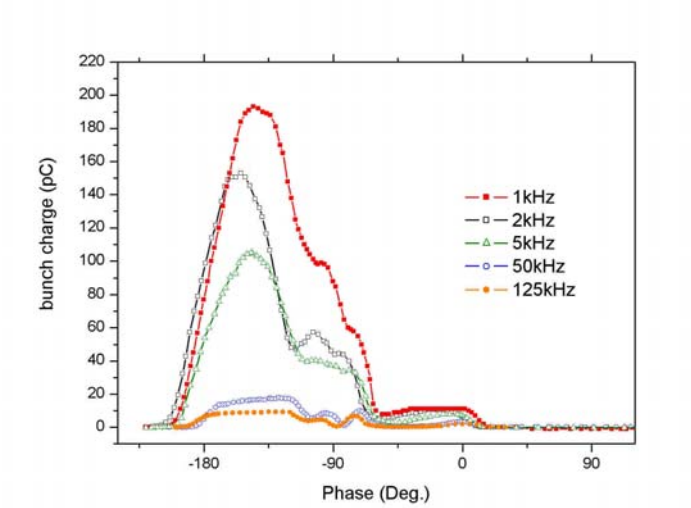

Fig. 6.9: Bunch charge versus launch phase for different laser repetition rates.

6.2 Space charge limitation

The space charge effect at the cathode is clearly visible in Fig. 6.10 where the maximum bunch charges obtained in the phase scan curves are shown as function of the corresponding laser pulse energy. The space charge becomes serious above 10 µJ resp. 150 pC. This space charge effect prevents that charge produced at the cathode increases linearly with the laser pulse energy. The situation can be improved by means of a higher acceleration field or a larger laser spot size.

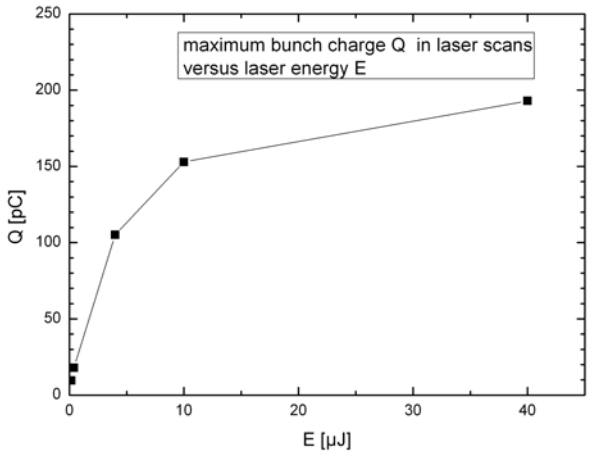

Fig. 6.10: Maximum bunch charge obtained in the laser phase scans as a function of laser pulse energy.

The space charge effect at higher bunch charges produces a beam hallo. Its appearance causes a beam loss which can be measured by a comparison of the beam current in the Faraday cup (0.6 m from gun) and in the beam dump (4 m from gun) for different bunch charges as it is shown in Fig. 6.11. At about 140 pC the dump current drops below the straight line (no beam loss).

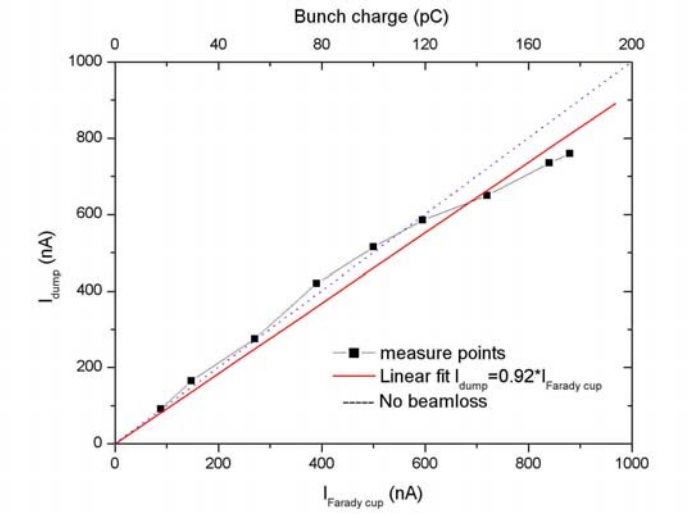

Fig. 6.11: Beam dump current versus Faraday cup current with increasing bunch charge obtained at a laser repetition rate of 5 kHz.

6.3 Energy and energy spread measurement

For energy and energy width measurement the 180° bending magnet of the diagnostic beam line has been used. The beam has been evaluated at screen DV05. As a reference serves screen DV04 which is in the straight beam line section behind the dipole magnet. Its optical path length is same as for screen DV05.

The beam energy as a function of launch phase is presented in Fig. 6.12. At the acceleration gradient of 5 MV/m the maximum beam energy is 2.06 MeV. The comparison with the laser phase scan in Fig. 6.4 shows that the energy drops down at phases > -160° whereas the emission current is still constant until -120°. The beam energy could be also determined for the additional peaks appear in the curve in Fig. 6.4. The beam energy in dependence on the acceleration gradient is shown in the Fig. 6.13.

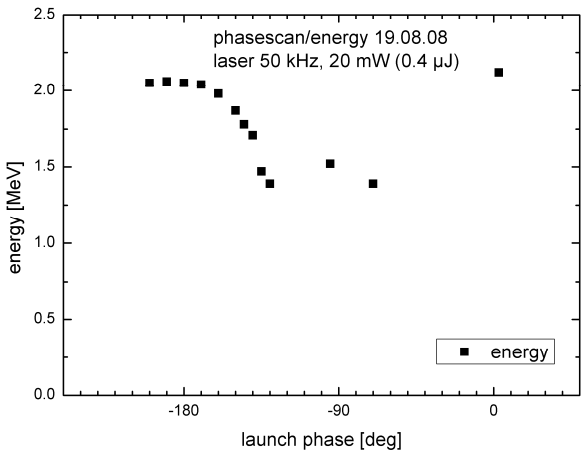

Fig. 6.12: Electron beam energy versus launch phase measured by means of the 180° bending magnet.

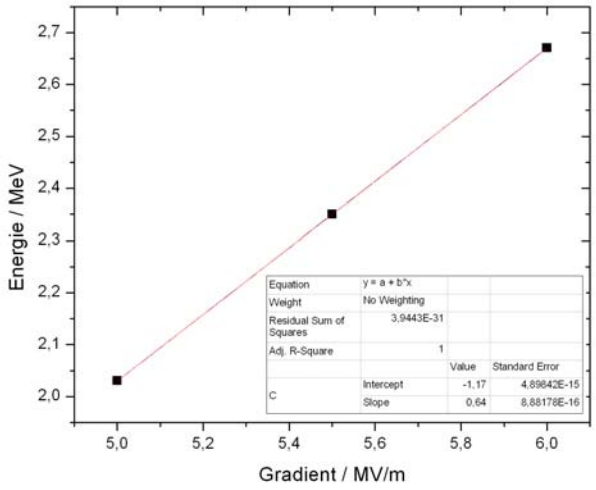

Fig. 6.13: Electron beam energy versus acceleration gradient.

For energy width measurement the screen DV05 was calibrated by changing the acceleration gradient. The measurement shown in Fig. 6.14 was carried out in a similar way as the laser phase scans, i.e. the laser pulse energy was constant while the launch phase was varied. Thus the bunch charge was not constant and has the dependence as shown in Fig. 6.4. But the minimum in the energy width of about 20 keV rms between –180° and –160° belongs to the bunch charge maximum and the region of highest electron energy.

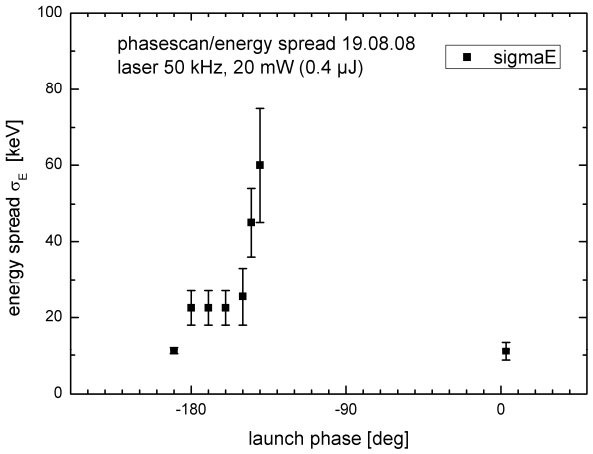

Fig. 6.14: Rms energy spread versus launch phase measured by means of the 180° bending magnet. The phase range from –180° to –150° belongs to bunch charges of about 15 pC.

For a fixed launch phase of -160° the electron energy and the energy spread was measured as a function of bunch charge (see Fig. 6.15). As expected the energy is independent of bunch charge. With exception for very low bunch charges (<5 pC) we found a nearly constant energy spread. The values of the energy spread are somewhat higher than in the previous measurement presented in Fig. 6.14.

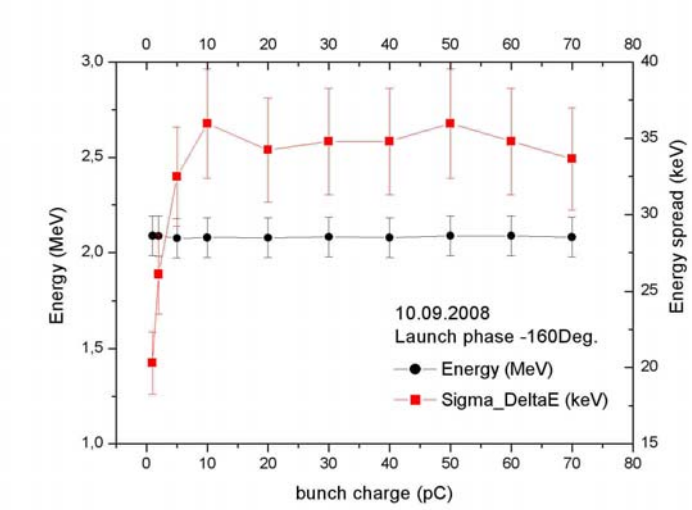

Fig. 6.15: Energy and rms energy spread versus bunch charge measured at a launch phase of –160°.

6.4 Transverse emittance

The transverse emittance measurements presented in the following have been carried out with the solenoid scan method. For these measurements the gun solenoid and the screens DV01 and DV02 have been used. Between the solenoid and the screens there is only a drift space of 38 cm and 170 cm, respectively. The quadrupoles in between were not used. The magnetic axial field distribution of the solenoid was precisely measured. Thus the focal strength in dependence on the excitation current I can be calculated. The measured beam size $\sigma^2_{x,y}$ on the screen is a parabolic function in I^2 containing the phase space ellipse parameters. From a quadratic fit these parameters and the emittance can be determined. It is well known that the solenoid/quadrupole scan method is not suitable for space charge dominated beams. Nevertheless, this method has been applied for first preliminary measurements. For the next beam time period in 2009 the slit mask method will be used. In Fig. 6.16 the evaluation software for the solenoid scan method is shown. In the diagram the square of the rms beam radius is plotted versus the solenoid current. The red curve is the least-square-fit to the measurement points.

In order to establish the operation phase of the gun, the tranverse emittance was measured as a function of laser phase as it is shown in Fig. 6.17. The bunch charge was 1 pC and the beam size was measured on screen 1 and 2, as well as in x- and y-direction. Considering also the results of the laser phase dependence in the energy and energy width measurements, the laser phase was set to -160°. For this laser phase the transverse emittance as a function of bunch charge has been measured. The results are shown in Fig. 6.18. The data analysis has been carried out for the second screen only. It requires less focusing and thus a lower space charge effect is expected. Measurements were carried out till 70 pC. For higher bunch charges the method could not be applied. The strong space charge effect causes a solenoid current dependence of the beam size which could not be fitted with the theoretical curve. Furthermore the beam shows an increasing halo. The figure shows only the data analysis from the second screen. Due to the longer distance the focusing was less strong and the space charge effect less pronounced. To measure the beam size CCD camera images with 8 bit and 660 x 495 pixel were produced, the camera gain was adapted, back ground subtracted and a region of interest (RoI) selected. In the RoI the beam spot size was obtained by direct rms analysis or by a Gaussian fit to projection profile. Both results are shown in Fig. 6.18.

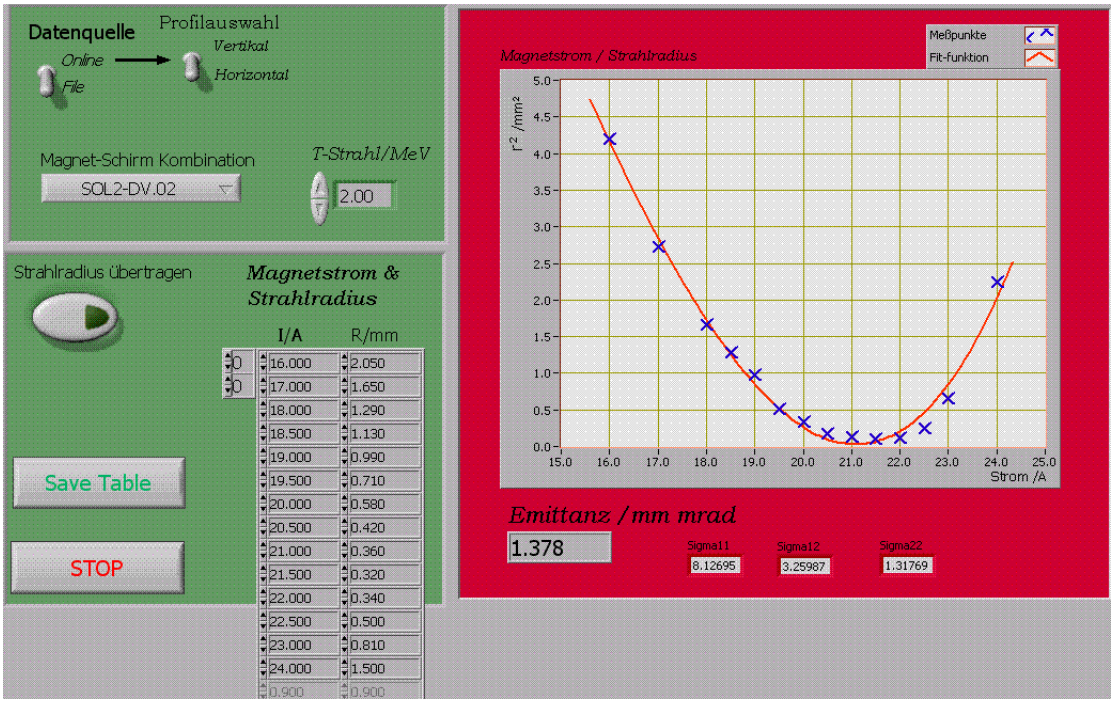

Fig. 6.16: LabView tool for the data analysis of the solenoid scan.

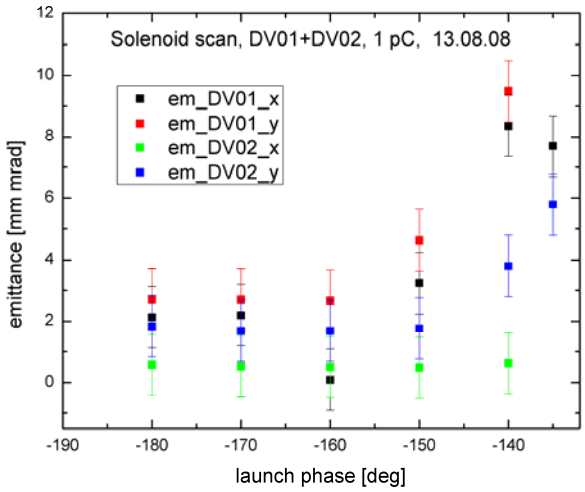

Fig. 6.17: Normalized rms transverse emittance for a bunch charge of 1 pC measured on screen 1 (DV01) and screen 2 (DV02) and in horizontal (x) and vertical (y) direction.

In Fig. 6.18 the blue curve shows the result of an ASTRA simulation with parameters which correspond to the present experimental situation. The peak value of the electric acceleration field was chosen to 15 MV/m, the cathode 2 mm retraced, the laser pulse was Gaussian with15 ps FWHM, the laser spot a radial flat top with 2.8 mm diameter, for the launch phase the optimum value was taken for each bunch charge. In the simulation bunches could be accelerated up to a bunch charge of about 100 pC. For higher bunch charges particle loss occurs due the space charge near the cathode. The transverse emittance starts with about 0.5 mm mrad and increases to about 7 mm mrad at 100 pC. This simulation agrees rather well

with the experimental data. Especially there is a good agreement in the predicted space charge limit.

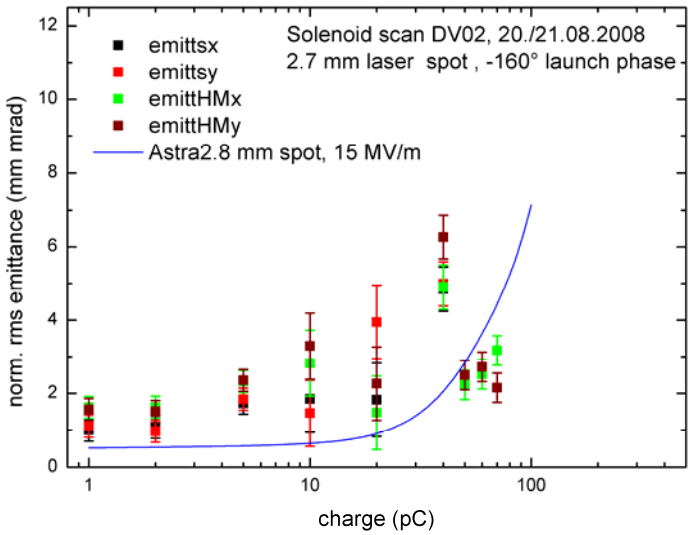

Fig. 6.18: Normalized rms transverse emittance as a function of bunch charge at a laser launch phase of -160° measured with the solenoid scan method using beam spot on screen DV02. Measurement in horizontal (x) and vertical (y) direction, direct rms beam spot size (emittHM) and Gaussian fit (emits).

6.5 Optimized Parameters for the SRF gun

For the next runs of the SRF gun in 2009 it is planned to deliver beam to the ELBE accelerator for user operation. Thereby it is important to deliver beam with bunch charges above 100 pC. It is obvious that the present low acceleration gradient of the gun is the crucial point. As reported in Section 3, the acceleration gradient could be increased to about 18 MV/m peak field by means of RF high power processing at the end of the run. Furthermore the space charge effect can be reduced by a larger laser spot size. Both changes can improve the beam parameters in comparison to those presented in this report. For a prediction ASTRA simulations have been carried out with 18 MV/m peak field. The cathode position, laser launch phase and laser spot size have been optimized. In Fig. 6.19 the results for the normalized transverse rms emittance versus bunch charge are presented. The figure shows for comparison the curve for the present gradient (15 MV/m peak field) and laser spot diameter of 2.8 mm (blue) as already presented in Fig. 6.16, the curve for 18 MV/m peak field and 2.8 mm laser spot (green), as well as the curve for 18 MV/m peak field and an optimized laser spot diameter of 5.2 mm (red). For the smaller laser spot the space charge at the cathode limits the bunch charge to 100 pC at present and to 200 pC for the 18 MV/m case. For the higher field and enlarged laser spot the space charge limit at the cathode is about 750 pC. Now the limitation is the transverse emittance. If a value of 10 mm mrad is acceptable, the bunch charge which can be used will be 500 pC.

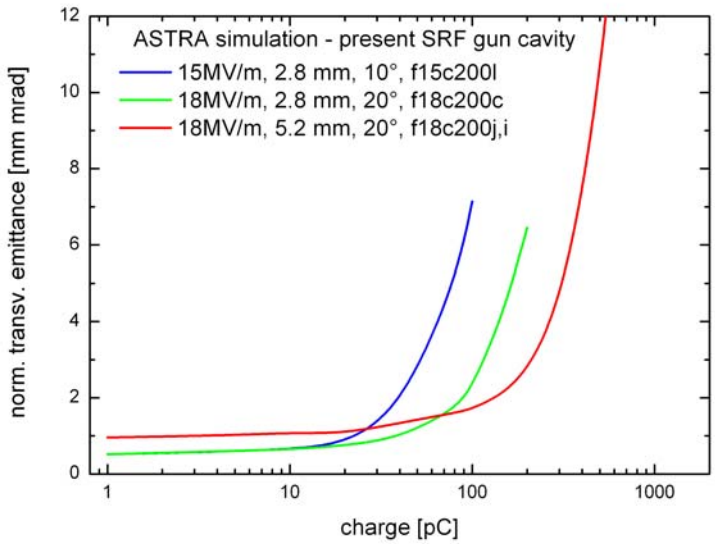

Fig. 6.19: ASTRA simulation of the normalized rms transverse emittance as a function of bunch charge for the SRF gun cavity for E_{peak} = 15 MV/m and d_{laser} = 2.8 mm as used in the present run (blue curve) and results expected for E_{peak} = 18 MV/m (green curve) and additionally d_{laser} = 5.2 mm (red curve) as planned for the next run.

7. Others

7.1 Multipacting

Inside the cells and the choke filter of the 3½-cell cavity multipacting does not occur. We observed multipacting in the coaxial channel formed by the circular opening in the half-cell backplane and the photo cathode stem during ramping up the RF gradient. The effect could be suppressed with a DC voltage applied to the photo cathode. It was found that the voltage which was needed depends on the cathode type. But in all cases this voltage does not exceed 5 kV.

7.2 Dark current

The dark current at 5 MV/m acceleration gradient was measured to about 5 nA. By means of the solenoid the dark current delivers an imaging of the photo cathode as shown in Fig. 7.1. The figure shows CCD camera pictures of YAG screen 1. A Cu cathode is inserted.

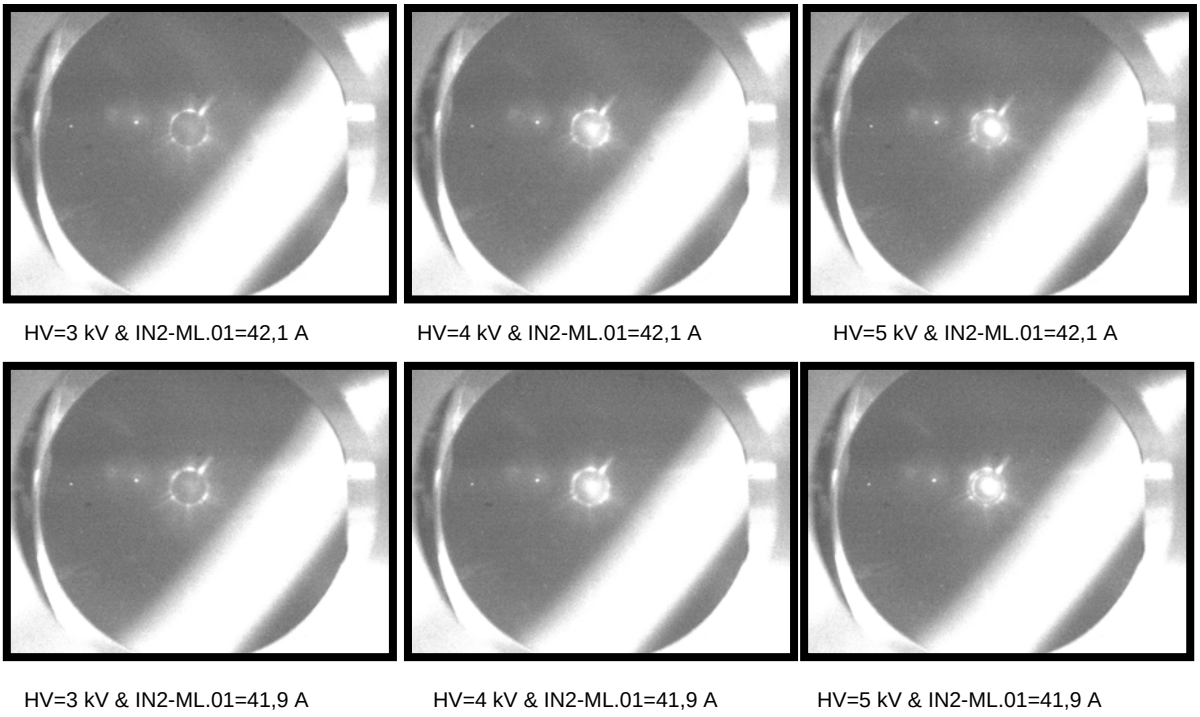

Fig. 7.1: Dark current images of the photo cathode using the solenoid for focusing.

8. Summary

- In November 2007 the first electron beam was generated from the superconducting RF photo electron gun. Since that time the gun has been in operation for about 500 hours without serious problem. Electron beam has been produced with a Cu photo cathode and with Cs_2Te photo cathodes. The gun was always operated in CW mode. The average beam current was about 1 μA.

- Cryogenic, radio frequency (cavity performance, pass band modes, field distribution, He-pressure sensitivity, Lorentz force detuning), and beam parameters (laser phase scan, beam energy, energy spread, transverse emittance) have been measured.

- The SRF gun has been operated with an acceleration gradient of 5 MV/m which belongs to a peak field of about 15 MV/m. The electron beam energy was 2.1 MeV.

- The cavity performance has been measured regularly. We did not observe any cavity degradation.

- Since May 2008 the gun has been operated with Cs_2Te photo cathodes. Due the insufficient vacuum in the transfer system the quantum efficiency was dropped down to about 0.1 % in the gun. An accidental venting in the summer shut-down destroyed the first Cs_2Te cathode after 44 h running time. The second Cs_2Te was used for about 250 h until the end of the beam time.

- Bunch charges up to 200 pC were produced. For bunch charges up to about 100 pC a electron beam of sufficient quality could be produced. The transverse emittance is about 1 mm mrad for small bunch charge and increases to about 6 mm mrad at the high bunch charge limit.

- A high power RF processing at the end of the measurement period improved the cavity performance. Thus the gun can be operated at 6.5 MV/m (3 MeV electron energy) in the next run.

- The expected operation with 3 MeV and an optimized laser spot diameter of 5.2 mm would allow bunch charges up to 500 pC.

- For the next run in 2009 it is intended to use the SRF gun as injector for ELBE and to operate the gun at high average current with a 30 kW IOT RF power source.

9. References

[1] P. Michel, et al., "The Rossendorf IR-FEL ELBE", Proc. FEL 2006, Berlin, Germany, p. 488.
[2] A. Arnold, et al., "Development of a Superconducting Radio Frequency Photo Electron Injector", Nucl. Instr. and Meth. A 577, 440 (2007).
[3] J. Teichert, et al. "Cryomodule and Tuning System of the Superconducting RF Photo-Injector", Proc. FEL 2006, Berlin, Germany, p 575.
[4] B. Aune, et al., "Superconducting TESLA Cavities", Phys. Rev. Special Topics AB 3**,** 092001 (2000).
[5] R. Xiang et al., CARE Report „Photocathode test in superconducting cavity", 2008.
[6] T. Kamps et al., "Electron beam diagnostics for a superconducting radio frequency photoelectron injector", Rev. Sci. Instrum. 79, 093301 (2008).

Acknowledgement

We acknowledge the support of the European Community-Research Infrastructure Activity under the FP6 "Structuring the European Research Area" programme (CARE, contract number RII3-CT-2003-506395) and the support of the German Federal Ministry of Education and Research grant 05 ES4BR1/8.